# Nanoscale

Accepted Manuscript


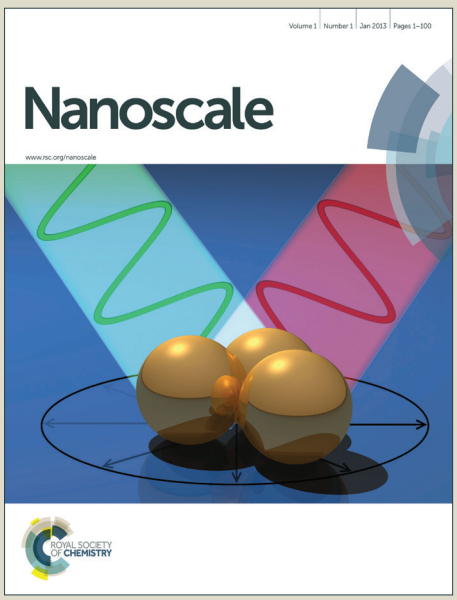





ROYAL SOCIETY OF CHEMISTRY

www.rsc.org/nanoscale

Cite this: DOI: 10.1039/c0xx00000x

www.rsc.org/chemcomm

COMMUNICATION

# Template-free construction of hollow α-$Fe_2O_3$ hexagonal nanocolumns particles with exposed special surface for advanced gas sensing properties

**Linqiang Sun,[a] Xiao Han,[a] Kai Liu,[a] Shan Yin,[a] Qiaoli Chen,[b] Qin Kuang,[b] Xiguang Han*[a], Zhaoxiong Xie[b], Chao Wang[a]**

***Received (in XXX, XXX) Xth XXXXXXXXX 2014, Accepted Xth XXXXXXXXX 2014***
**DOI: 10.1039/b000000x**

**Hollow α-$Fe_2O_3$ hexagonal nanocolumns particles (HHCPs) with exposed (10$\bar{1}$0) and (11$\bar{2}$5) facets have been synthesized through a hydrothermal method in the absence of templates. The time-dependent experimental results demonstrate that the formation of HHCPs includes four main steps: (1) formation of nanowire precursors, (2) aggregation and conversion to $Fe_{1.833}(OH)_{0.5}O_2$ solid ellipsoid particles (SEPs), (3) dehydration to form hollow ellipsoid particles (HEPs), (4) recrystallization to HHCPs. Due to their advantages of the hollow structure and special surface exposed external and internal on pore structure, the HHCPs exhibit higher gas sensing than that of calcinated SEPs (CSEPs) and HEPs.**

Due to low cost, easy production and simple measuring electronics, metal oxide-based gas sensor are predominant in the aspects of solid-state gas detecting devices.[1] However, it is still a great obstacle for gas sensors based on bulk materials with low surface area to improve gas sensing properties in sensitivity, selectivity and response speed. Hollow and porous oxide structures have advantages for gas senesing application, such as large surface area and favorable for gas diffusion.[2] Therefore, on the design of metal oxide nanomaterials with appropriate porosity have recently attracted much attention because of their potential application in gas sensing. For example, Chen group developed a facile solution-based method to synthesize hollow $Cu_{2-x}Te$ nanocrystals based on the kirkendall effect and their enhanced CO gas-sensing properties.[2c]

The detection mechanism of metal oxides-based gas sensors is the reaction between the adsorbed oxygen on the surface of materials and the target molecules.[3] Therefore, the sensitivity and selectivity of the gas sensors are connected with the density of active site on the surface of materials which could adsorb oxygen and target gases. Anisotropy is a basic property of single crystal. Various facets or surfaces have different surface atomic arrangement and dangling bonds, result in form different active site.[4] Considering the fact that the surfaces of particles on the nanoscale become dominant, control the surfaces of nanoparticles presents an important direction for improving the gas-sensing property.[5] For example, Xie group reported that α-$Fe_2O_3$ nanocrystals with different exposed facets from {012} facets to {113} facets and {001} facets have been successfully synthesized under surfactant–free condition by hydrothermal process, and the nanocrystals enclosed with {113} facets exhibit higher gas sensing ability.[5c] Based on the above analysis, both the hollow structure and surface structure can influence the sensitivity and selectivity of the gas sensors. Therefore, combining the hollow structure and special surface exposed external and internal on pore structure into one nanomaterial will further improve the gas sensing properties.

Hematite (α-$Fe_2O_3$), an n-type semiconductor (Eg = 2.1 eV), is believed to a promising materials for Li-ion battery, gas sensors and so on, because of the features of non-toxicity, low cost, high stability and environmental compatibility.[6] Recentaly, α-$Fe_2O_3$ nanoparticles with porous walls or hollow cavities are particularly desirable for improved sensing performance.[7] However, most of the synthesized α-$Fe_2O_3$ hollow structure are spheres shape or other irregular morphologies without special facets exposed.[6a-c, 7] Therefore, it is a great challenge and opportunity to synthesize α-$Fe_2O_3$ hollow structure with exposed special surface to further improve the gas sensing properties.

Herein we report a facile hydrothermal method to synthesize the hollow α-$Fe_2O_3$ hexagonal nanocolumns particles (HHCPs) with exposed external and internal (10$\bar{1}$0) and (11$\bar{2}$5) facets on pore structure in the mixture of water and ethanol systems (see Supporting information). Fig. 1a shows the powder X-ray diffraction (PXRD) pattern of the product, where all the characteristic diffraction peaks of the product match well with the rhombohedral α-$Fe_2O_3$ with the

[a]*Jiangsu Key Laboratory of Green Synthetic Chemistry for Functional Materials, Department of Chemistry, School of Chemistry and Chemical Engineering, Jiangsu Normal University, Xuzhou, 221116 (P. R. China) E-mail: xghan@jsnu.edu.cn*
[b]*State Key Laboratory of Physical Chemistry of Solid Surfaces & Department of Chemistry, College of Chemistry and Chemical Engineering, Xiamen University, Xiamen 361005, China*
† Electronic Supplementary Information (ESI) available. Detailed synthesis procedure and some experimental results see DOI: 10.1039/b000000x.

cell constants of a = 5.028 Å and c = 13.730 Å (JCPDS No: 00-001-1053). No impurity peaks observed and the diffraction peaks are comparatively sharp, suggesting that the as-synthesized α-$Fe_2O_3$ have good crystallinity. Field-emission scanning electron microscopy (FESEM) and transmission electron microscopy (TEM) studies reveal the morphology and detailed structure of the products. A panoramic FESEM image (Fig. 1b) shows that the sample consists of uniform nanocolums with size of about 200 nm in length and 150 nm in width. The higher magnification SEM (insert of Fig. 1b) clearly shows the cuspate tips and hollow interior cavities. Further TEM observation (Fig. 1c) and selected-area electron diffraction (SAED) (Fig. 1d) indicate that the single α-$Fe_2O_3$ HHCP displays a hexagonal ring projection profile with angle of 120° under electron beam along the [001] zone axis. The profile and angles agree well with the model of an ideal cuspate tip hexagonal colum enclosed by $\{10\bar{1}0\}$ on the sides and $\{11\bar{2}5\}$ facets on the tip projected along the [001] zone axis (Fig. 1f). The SAED pattern also indicates the single-crystalline characteristic of the HHCP. Fig. 2e shows the high-resolution TEM (HRTEM) image of marked in Fig. 2c, where the (100) lattice fringes (2.5 Å) can be clearly observed. To further confirm the indentity of the exposed surfaces of the HHCPs, another particle projected from the [100] zone axis is observed by TEM (Fig. 1g) and SAED pattern (Fig. 1h). As shown in Fig. 1g and j, both the outline and the apex angle of the particle still correspond well with the ideal HHCP model the [100] zone axis. On the basis of the above SEM, TEM observations and structural analyses, we conclude that the exposed surfaces of the as-prepared HHCPs are the $\{10\bar{1}0\}$ and $\{11\bar{2}5\}$ facets.

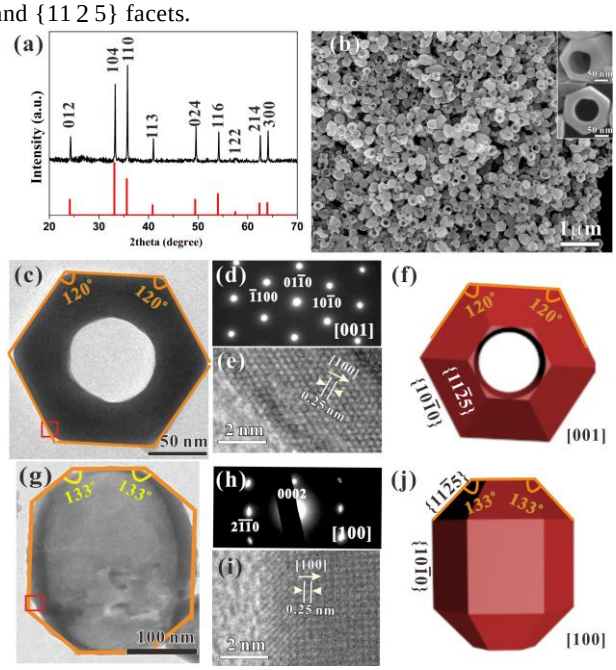


**Fig 1.** (a) Standard and observed XRD patterns of the product; (b) SEM images of the as-prepared hollow hexagonal column particles (HHCPs), upper inset show the corresponding enlarged images; (c) TEM image of individual HHCP viewed along the [001] direction; (d) the SAED pattern corresponding to c; (e) HRTEM image of the portion marked in (c); (f) the ideal geometrical model of individual HHCP projected from [001] direction; (g) TEM image of individual HHCP viewed along the [100] direction; (h) the SAED pattern corresponding to (g); (i) HRTEM image of HHCP marked in (g); (j) Model of an ideal HHCP projected from the [100] direction.

To understand the formation mechanism of the HHCPs, their growth process is followed by examining the products obtained at different intervals of reaction time. At the early stage of the reaction (15 min), the XRD pattern (Fig. 2a, 15min) and thermal gravimetric analysis (TGA) (Fig. S2a) indicate that the products are amorphous precursor. The SEM image shows that some wire-like precursor are formed (Fig. 2b), and FTIR spectroscopy indicates the surface adsorb of sodium dodecylbenzenesulfonate (SDBS) (Fig. S1). When the reaction time is extended to 30 min, some amorphous wire-like precursor have been aggregated to solid ellipsoid particles (SEPs) (Fig. 2c). After 1 h, all the amorphous precursor have grown to SEPs (Fig. 2d). A typical powder X-ray diffraction (PXRD) pattern of the as-prepared products which can be indexed to the Rhombohedral phase of $Fe_{1.833}(OH)_{0.5}O_{2.5}$nanoparticles with cell constants of a = 5.034 Å, b = 5.034 Å, c = 13.750 Å, α = 90°, β = 90°, γ = 120° (PDF No. 01-076-0182). To further demonstrate the ingredient of SEPs (60 min), the thermal gravimetric analysis was carried out (Fig. S2b), the total weight loss in the decomposition process is about 2.8%，which agrees with the theoretical calculating value of 2.98%. The sample after TGA has been characterized by SEM (Fig. S3), the morphology of sample still keep the solid ellipsoid shape (the obtained products defined as CSEPs). The hollow α-$Fe_2O_3$ ellipsoid particles (HEPs) can be observed at 2 h shown in Fig. 2e. When the reaction time is further prolonged to 6h, the hollow α-$Fe_2O_3$ hexagonal nanocolumns particles HHCPs have been observed.

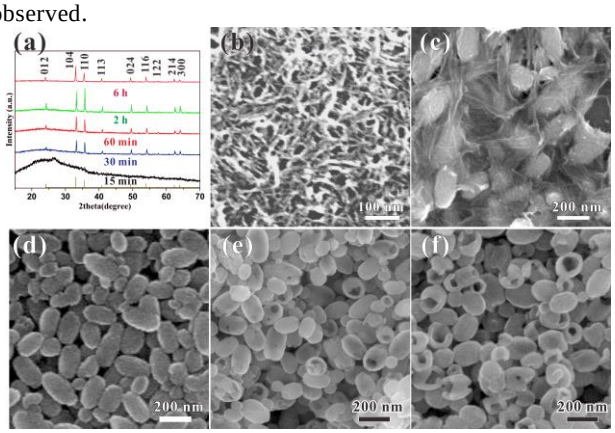


**Fig. 2.** (a) Typical XRD pattern of the product obtained from different reacted time; (b-f) the SEM images of the products obtained from different reaction time, (b) 15 min; (c) 30 min; (d) 60 min; (e) 2 h; (f) 6 h.

**Scheme 1.** Schematic representation of the formation of HHCPs.

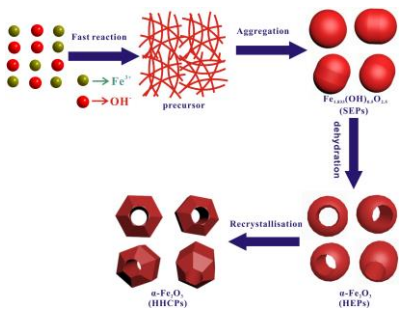

On the basis of the time-dependent experiments, the possible formation process of HHCPs is reasonably illustrated in Scheme 1. The formation of HHCPs could be described as a four-steps procedure. In the first step, when the reacted system is mixed with $Fe^{3+}$ and $OH^-$ under the appropriate reaction conditions, the amorphous precursors have been fast formed. Due to the exist of SDBS, the morphology of the amorphous precursor is prone to line-like structure. In order to reduce the surface energy, the line-like structures further agglomerate to construct $Fe_{1.833}(OH)_{0.5}O_2$ solid ellipsoid particles (step two). With increasing the reacted time and temperature, most of amorphous precursor gradually generate $Fe_{1.833}(OH)_{0.5}O_2$ nanoparticles, and then the $Fe_{1.833}(OH)_{0.5}O_2$ precuresor dehydrate into $\alpha$-$Fe_2O_3$ nanoparticles. In the process of dehydration, the surface of precuresor were easily first dehydrated to form the $\alpha$-$Fe_2O_3$. Taking the $\alpha$-$Fe_2O_3$ on the surface as the "hard-template", and then the internal component (including $Fe_{1.833}(OH)_{0.5}O_2$ and amorphous precursor) were also gradually dehydrate to form the hollow ellipsoid particles (HEPs) (step three). It is noteworthy that the surface of the final HHCPs is smoother, and the morphology is more regular than those of the SEPs and HEPs, which indicates that the recrystallization process have been in progress (step four).

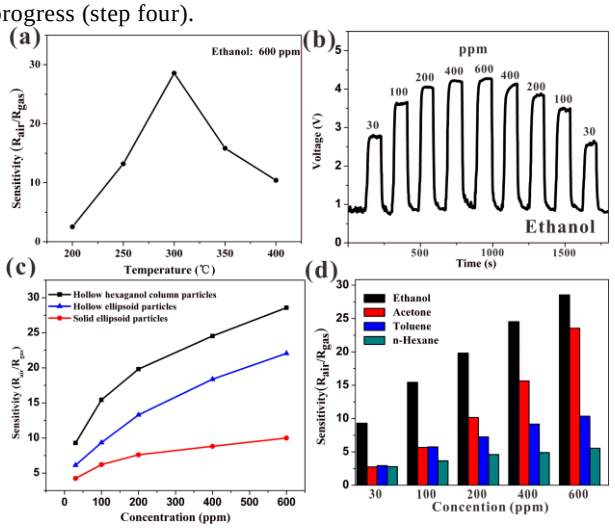


**Fig. 3.** (a) Operating temperature-dependent sensitivity curve of the HHCPs sensor in the presence of 600 ppm ethanol; (b) Dynamic sensing curve of the HHCPs sensor in using ethanol with different concentrations; (c) Concentration dependent sensitivity curves of three different samples; (d) Comparison between concentration-dependent sensitivities of HHCPs using different gases.

Based on the metal oxide gas sensing mechanism, the surface structures including exposed facets and their surface area have been domonstrated to greatly affect the performance of gas sensing application. Therefore, HHCPs with hollow structure and exposed with special surface expect to exhibit higher gas sesing ability. For evaluating the performance of HHCPs as sensing materials, ethanol was chosen as a target molecule. In order to find the optimal operating temperature, the sensing of the HHCPs snesor to 600 ppm of ethanol gas was measured at different operating temperatures ranging from 200 to 400 °C. As shown in Fig. 3a, the best operating temperature of the sensor is 300 °C consistent with most $Fe_2O_3$ nanostructure-based sensors in the literature.[8] Fig. 3b shows the dynamic sensing curve of the HHCPs measured at the optimal operating temperature, which clearly shows the response-recovery performances of the sensor. Noticeably, HHCPs sensor shows a very stable signal with on/off phenomenon when switching between air and ethanol. It also indicates that the response and recovery of the HHCPs sensor are less than 10s, which is favorable for the rapid detection of ethanol. Considering its internal hollow structure and special crystal facets exposed, the fast response and recovery of the HHCPs sensor should be attributed to the shortened diffusion path of the target molecule to the surface of the adsorption site. To confirm this result, the concentration-dependent sensitivities of HHCPs, HEPs and CSEPs were systematically compared, and the results are shown in Fig. 3c. The sensitivities of all the sensors increase with the detected gas concentrations. At the same gas concentration, HHCPs (hollow strucure and with exposed special facets) exhibit highest sensitivity, followed by HEPs (hollow structure) and CSEPs (calcination solid structure). The hollow structure shortened diffusion path of the target molecule to the surface and the special surface result in the more active site on the surface, thereby giving rise to better sensing performance. Gas selectivity is another key parameter for gas sensor. Fig. 3d compares sensitivity of the HHCPs snesor upon exposure to different concentrations of ethanol, acetone, toluene and hexane. By contrast, the HHCPs sensors exhibit remarkable selectivity to ethanol.

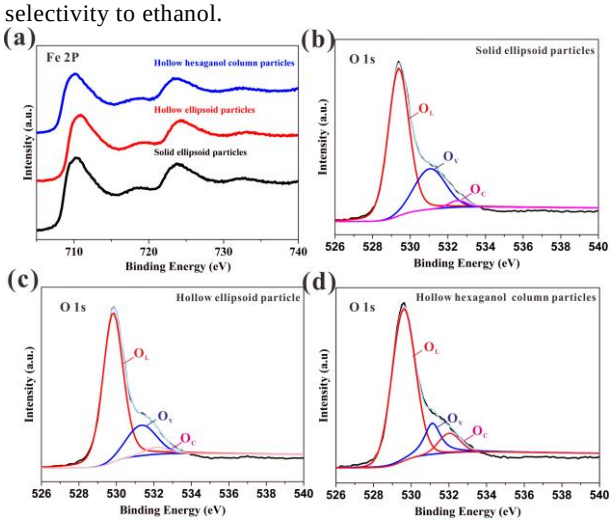


**Fig. 4.** (a) XPS spectra of Fe 2p of three different samples; XPS spectra and curve-fitting of O1s in (b) CSEPs; (c) HEPs; (d) HHCPs.

Table 1. Results of Curve Fitting of O1s XPS spectra of the different $Fe_2O_3$ Samples

| $Fe_2O_3$ samples | Fe $2p_{3/2}$ | Fe $2p_{1/2}$ | $O_L$ (Zn-O) | $O_V$ (vacancy) | $O_C$ (chemisirbed) |
|---|---|---|---|---|---|
| HHCPs | 710.2 | 723.5 | 529.6<br>76.7% | 531.5<br>14.6% | 532.1<br>8.7% |
| HEPs | 710.7 | 724.1 | 529.8<br>74.9% | 531.3<br>21.3% | 532.1<br>3.8% |
| CSEPs | 710.2 | 723.8 | 529.3<br>71.3% | 531.1<br>26.3% | 532.7<br>2.4% |

Recent studies reveal that the surface structures might be

the essential factor to determine the efficiency of gas sensing property. In order to obtain useful information about surface structures of three different shapes of samples, XPS analyses are used. Fig. 4a shows Fe 2p XPS spectra of HHCPs, HEPs and CSEPs for comparison. It is found that the Fe 2p XPS peaks of three samples are analogous for their position and distribution. However, there are some slight differences between O1s XPS peaks of three $Fe_2O_3$ samples, which are asymmetrical and present a visible shoulder. As shown in Fig. 4 b-d, each asymmetric O1s peak can be decomposed into three Gaussian components centered. The $O_L$ component of O1s spectrum centered at 529 eV is attributed to the lattice oxygen in the $Fe_2O_3$ phase, the $O_V$ component at the medium binding energy (531 eV) is associated with $O^{2-}$ ions in oxygen-deficient regions within the matrix of $Fe_2O_3$, and the $O_C$ component (532 eV) is usually attributed to chemisorbed and dissociated oxygen species($O_2^-$, $O^{2-}$, $O^-$) and $OH^-$. Therefore, we can estimate the oxygen-chemisorbed ability of three different samples according to the intensity of $O_C$ component in the O1s XPS peak. As shown in Table 1, the relative percentages of the $O_C$ component in three different samples are about 8.7% (HHCPs), 3.8% (HEPs) and 2.4% (CSEPs), respectively. Obviously, HHCPs with hollow structure and exposed with special surface are able to absorb more oxygen species than the HEPs with hollow structure and CSEPs with solid structure. The results of chemisorbed ability of these $Fe_2O_3$ samples are consistent with that of their gas sensing abilities, which adequately demonstrates that the gas sensing properties of $Fe_2O_3$ are closely related to the crytal surface and hollow structure.

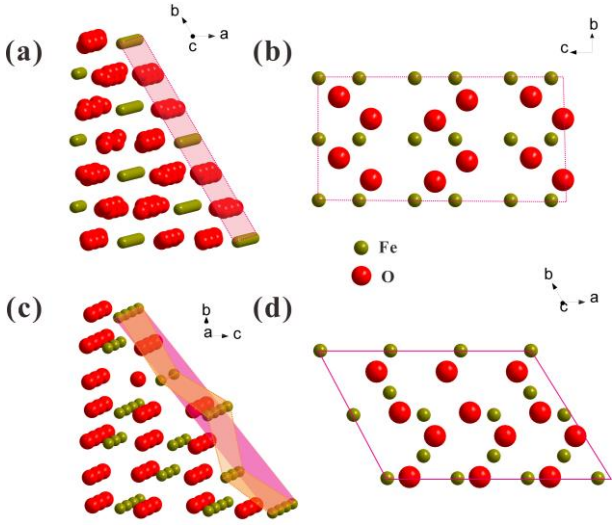


**Fig. 5.** Surface atoms arrange of (a-b) $\{10\bar{1}0\}$ facet; (c-d) $\{11\bar{2}5\}$ facet.

The surface atomic structures should paly an important role in determining the ability to absorb the oxygen species (such as $O_2^-$, $O^{2-}$, $O^-$, $OH^-$) and target molecules. Fig. 5 shows schematic models of $Fe_2O_3$ $\{10\bar{1}0\}$ and $\{11\bar{2}5\}$ surfaces. As shown in Fig. 5a, b, the $Fe_2O_3$ $\{10\bar{1}0\}$ surface contains several unsaturated Fe atoms. On the $\{11\bar{2}5\}$ surfaces (Fig. 5c, d), there are also some unsaturated Fe atoms, furthermore, it also has some step sites on the surface. The unsaturated Fe atoms and step sites are highly active in adsorption of ionized oxygen species, which will greatly improve the response of $Fe_2O_3$ to the detected gases. Due to the regular hollow structure, the internal surface of the HHCPs may also is the same surface structure as the external surface. Furthermore, the hollow structure also increase the BET surface of the particles (HHCPs (12.81 $m^2 \cdot g^{-1}$), HEP (11.51 $m^2 \cdot g^{-1}$), CSEP (9.77 $m^2 \cdot g^{-1}$), see Fig. S4). Therefore, the hollow structure increase the active surface area. The discussion above accounts for the high performance of as-prepared HHCPs with hollow structure and exposed with special surface comparison wih HEPs and CSEPs.

In conclusion, we have successfully prepared $\alpha$-$Fe_2O_3$ HHCPs with hollow structure and exposed with $\{10\bar{1}0\}$ and $\{11\ \bar{2}\ 5\}$ surfaces throught a template-free hydrothermal method. According to the time-dependent experimental results, we deduce that that the formation of HHCPs includes four main steps: (1) formation of precursors nanowires, (2) aggregation to $Fe_{1.833}(OH)_{0.5}O_{2.5}$ solid ellipsoid particles (SEPs), (3) dehydration to form hollow ellipsoid particles (HEPs), (4) recrystallisation to HHCPs. Due to the hollow structure and special crystal exposed, the HHCPs exhibit high gas sensing ability. More study on this nanomaterial is underway and its potential applications in fields such as photocatalysis and battery will be presented in the follow-up research. Due to the special structure, HHCPs are also likely to exhibit outstanding performance in photocatalysis, battery and so on.

This work was supported by the National Natural Science Foundation of China (Grant No. 21201088, 21333008, 21473081), the Qing Lan Project and the Project Funded by the Priority Academic Program Development of Jiangsu Higher Education Institutions.

## References

(1) (a) R. A. Potyrailo, V. M. Mirsky, *Chem. Rev.* 2008, **108**, 770; (b) M. E. Franke, T. J. Koplin, U. Simon, *Small* 2006, **2**, 36; (c) A. Tricoli, M. Righettoni, A. Teleki, *Angew. Chem. Int. Ed.* 2010, **49**, 7632.

(2) (a) J. H. Lee, *Sens. Actuators B Chem.* 2009, **140**, 319; (b) H. K. Wang, A. L. Rogach, *Chem. Mater*. 2014, **26**, 123; (c) G. J. Xiao, Y. Zeng, Y. Y. Jiang, J. J. Ning, W. T. Zheng, B. B. Liu, X. D. Chen, G. T. Zou, B. Zou, *Small* 2013, **9**, 793 (d) J. S. Chen, X. W. Lou, *Small* 2013, **9**, 1877; (e) Y. Y. Lü, W. W. Zhan, Y. He, Y. T. Wang, X. J. Kong, Q. Kuang, Z. X. Xie, L. S. Zheng, *ACS Appl. Mater. Interfaces* 2014, **6**, 4186.

(3) (a) N. Barsan, U.Weimar, *J. Phys. Condens. Matter*. 2003, **15**, R813; (b) A. Gurlo, R. Riedel, *Angew. Chem. Int. Ed.* 2007, **46**, 3826.

(4) (a) N. Tian, Z. Y. Zhou, S. G. Sun, Y. Ding, Z. L. Wang, *Science* 2007, **316,** 732; (b) A. R. Tao; S. Habas, P. D. Yang, *Small* 2008, **4,** 310; (c) Y. N. Xia, Y. J. Xiong, B. Lim, S. E. Skrabalak, *Angew. Chem., Int. Ed*. 2009, **48,** 60; (d) K. B. Zhou, Y. D. Li, *Angew. Chem., Int. Ed*. 2012, **51,** 602; (e) M. H. Huang, P. H. Lin, *Adv. Funct. Mater.* 2012, **22,** 14; (f) M. R. Gao, Y. F. Xu, J. Jiang, S. H. Yu, *Chem. Soc. Rev*. 2013, **42,** 2986; (g) H. G. Yang, C. H. Sun, S. Z. Qiao, J. Zou, G. Liu, S. C. Smith, H. M. Cheng, G. Q. Lu, *Nature* 2008, **453,** 638; (h) X. W. Xie, Y. Li, Z. Q. Liu, M. Haruta, W. J. Shen, *Nature* 2009, **458,** 746; (i) X. G. Han, Q. Kuang, M. S. Jin, Z. X. Xie, L. S. Zheng, *J. Am. Chem. Soc*. 2009, **131,** 3152.

(5) (a) X. G. Han, M. S. Jin, S. F. Xie, Q. Kuang, Z. Y. Jiang, Y. Q. Jiang, Z. X. Xie, L. S. Zheng, *Angew. Chem. Int. Ed*. 2009, **48,** 9180. (b) X. G. Han, H. Z. He, Q. Kuang, X. Zhou, X. H. Zhang, T. Xu, Z. X. Xie, L. S. Zheng, *J. Phys. Chem. C* 2009, **113**, 584; (c) J. J. Ouyang, J. Pei, Q. Kuang, Z. X. Xie, L. S. Zheng, *ACS Appl. Mater. Interfaces* 2014, **6**, 12505.

(6) (a) L. L. Li, H. B. Wu, L. Yu, S. Madhavi, X. W. Lou, *Adv. Mater. Interfaces* 2014, DOI: 10.1002/admi.201400050; (b) G. X. Gao, L. Yu, H. B. Wu, X. W. Lou, *Small* 2014, **10**, 1741; (c) Z. Y. Wang, D. Y. Luan, S. Madhavi, Y. Hu, X. W. Lou, *Energ. Environ. Sci.* 2012, **5**, 5252; (d) X. L. Li, W. J. Wei, S. Z. Wang, L. Kuai, B. Y. Geng, *Nanoscale* 2011, **3**, 718; (e) S. Agarwala, Z. H. Lim, E. Nicholson, G. W. Ho, *Nanoscale* 2012, **4**, 194; (f) J. M. Ma, L. Mei, Y. J. Chen, Q. H. Li, T. H. Wang, Z. Xu, X. C. Duan, W. J. Zheng, *Nanoscale* 2013, **5**, 895; (g) J. S. Chen, T. Zhu, X. H. Yang, H. G. Yang, X. W. Lou, *J. Am. Chem. Soc.* 2010, **132**, 13162; (h) L. Zhang, H. B. Wu, S. Madhavi, H. H. Hng, X. W. Lou, *J. Am. Chem. Soc.* 2012, **134**, 17388; (i) L. Zhang, H. B. Wu, X. W. Lou, *J. Am. Chem. Soc*. 2013, **135**, 10664.

(7) (a) Y. Wang, J. L. Cao, S. R. Wang, X. Z. Guo, J. Zhang, H. J. Xia, S. M. Zhang, S. H. Wu, *J. Phys. Chem. C* 2008, **112**, 17804; (b) J. Ming, Y. Q. Wu, L. Y. Wang, Y. C. Yu, F. Y. Zhao, *J. Mater. Chem.* 2011, **21**, 17776; (c) S. Wang, L. W. Wang, T. L. Yang, X. H. Liu, J. Zhang, B. L. Zhu, S. M. Zhang, W. P. Huang, S. H. Wu, *J. Solid State Chem*. 2010, **183**, 2869.

(8) (a) J. J. Ouyang, J. Pei, Q. Kuang, Z. X. Xie, L. S. Zheng, *ACS Appl. Mater. Interfaces* 2014, **6**, 12505; (b) H. T. Fan, T. Zhang, X. J. Xu, N. Lv, *Sens. Actuators B* 2011, **153**, 83

*Graphical Abstract*

Hollow α-$Fe_2O_3$ hexagonal nanocolumns particles (HHCPs) with exposed $\{10\bar{1}0\}$ and $\{11\bar{2}5\}$ facets have been prepared through a hydrothermal method in the absence of template. Due to their advantages of the hollow structure and special surface exposed external and internal on pore structure, it exhibits higher gases sesning capacity than hollow ellipsoid particles (HEPs) and calcination solid ellipsoid particles (CSEPs).